Contributions of C-Band SAR Data and Polarimetric Decompositions to Subarctic Boreal Peatland Mapping

Michael A. Merchant, Justin R. Adams, Aaron A. Berg, Jennifer L. Baltzer,
William L. Quinton, and Laura E. Chasmer

Abstract—The objective of this paper is to assess the accuracy of C-band synthetic aperture radar (SAR) datasets in mapping peatland types over a region of Canada's subarctic boreal zone. This paper assessed contributions of quad-polarization linear backscatter intensities ($\sigma°$HH, $\sigma°$HV, $\sigma°$VV), image textures, and two polarimetric scattering decompositions: 1) Cloude–Pottier, and 2) Freeman–Durden. Four quad-polarimetric RADADSAT-2 images were studied at incidence angles of 19.4°, 23.1°, 45.8°, and 48.1°. The influence of combining dual-angular information acquired within a short temporal span was also assessed. These C-band SAR data were used to classify peatlands according to isolated flat bogs (bogs), channel fens (fens), raised peat plateaus (plateaus), and forested uplands (uplands) using a supervised support vector machine (SVM) classifier. Numerous classifications were examined to compare the unique contributions of these variables to classification accuracy. Results suggest linear backscatter variables in isolation produce comparable classification results with those of the Freeman–Durden and Cloude–Pottier decompositions. Combining polarimetric decomposition and texture data into classifications with linear backscatter data resulted in only minor ($\sim$1–3%) improvement. Combining classifications from small and large incidence angles (dual-angular) significantly improved classification results over those of a single image. Classification accuracy was the highest for isolated bogs and open water surfaces, whereas fens, uplands, and plateaus had lower accuracies. The highest accuracy classification (84% and kappa coefficient of 0.80) used a dual-angular approach, with additional decomposition and texture information. However, it is noted that texture information rarely improved classification results across all tests. This approach identified isolated flat bogs, channel fens, and raised peat plateaus with >76% producer's accuracies.

Index Terms—Image classification, peatlands, polarimetric radar, synthetic aperture radar (SAR).

M. A. Merchant is with Ducks Unlimited Canada, Boreal Program, Edmonton, AB T6S 1L6, Canada (e-mail: m_merchant@ducks.ca).

J. R. Adams, J. L. Baltzer, and W. L. Quinton are with the Cold Regions Research Centre, Wilfrid Laurier University, Waterloo, ON N2L 3C5, Canada (e-mail: jadams@wlu.ca; jbaltzer@wlu.ca; wquinton@wlu.ca).

A. A. Berg is with the Department of Geography, University of Guelph, Guelph, ON N1G 2W1, Canada (e-mail: aberg@uoguelph.ca).

L. E. Chasmer is with the Department of Geography, University of Lethbridge, Lethbridge, AB T1K 6T5, Canada (e-mail: laura.chasmer@uleth.ca).

I. INTRODUCTION

PEATLANDS play several functionally important roles at the regional and global scales due to their controls on biological, ecological, and hydrological processes. For example, peatlands recycle nutrients and purify water resources, both of which are critical in the functioning and preservation of sensitive ecosystems. Peatlands, on average, have also been a net sink of atmospheric greenhouse gases over thousands of years [1], making them an immense store of ancient carbon and methane. However, boreal peatlands, specifically those at the southern margin of the discontinuous permafrost zone (DPZ), have recently undergone rapid permafrost loss and dramatic land cover changes concomitant with a warming climate [2]–[5].

Permafrost thaw in these environments is very concerning, as even small disturbances within the DPZ have the potential to transform peatlands from atmospheric sinks into sources [6], [7]. For example, using aerial photographs and high-resolution optical satellite imagery dating from the 1940 s to 2000, Beilman and Robinson [8] found permafrost areal extent losses of 50% and 33% at two peatland sites within the DPZ (Trout Lake and Liard River, Northwest Territories). This quantified loss of permafrost aligns strongly with the warming trend that has occurred over the northern hemisphere [9]. More specifically, Quinton *et al*. [4] show that mean annual air temperature measured at Fort Simpson, Northwest Territories, has increased from -4.1 °C during 1896–1970, to -3.2 °C during 1971–2000, and to -2.3 °C during 2001–2007. Consequently, accelerated permafrost thaw from amplified climate warming is affecting the flux and storage of water from major land cover types, as each performs unique hydrological functions [10]–[12]. As peatland hydrology is largely connected to vegetation communities and the extent of the underlying active layer, changes such as alterations to water storage pathways [13] and deepening of the active layer [12] are predicted to drive large-scale changes in ecosystem functions, such as carbon sequestration and biogeochemical cycling [14]–[16]. This makes monitoring the rate and spatial pattern of land cover change in this region a significant task as continued warming is predicted over the coming decades [17]. However, the extremely vast spatial extents of these sensitive ecosystems, their relative inaccessibility, and their heterogeneous land covers necessitate the development of remote sensing monitoring techniques.

Techniques involving synthetic aperture radar (SAR) have demonstrated great potential for mapping peatland spatial extent and types [18]–[22]. Spaceborne SAR sensors hold several advantages over multispectral data for mapping peatland complexes in northern hemisphere environment. SAR is favorable because of the sensitivity of microwaves to surface hydrology conditions as well as the condition and physical geometry of vegetation. SAR sensors also operate independent of solar illumination or cloud presence. Depending on the sensor and mode of acquisition, SAR imagery can be acquired at relatively fine resolutions (e.g., 10 s of m or less), which is valuable for mapping localized vegetation change and the small-scale fractionation of peatland cover type. Previous and current Earth observation satellites equipped with SAR, such as ERS-1/2, JERS-1, ENVISAT ASAR, and RADARSAT-1/2, offer(ed) a range of image resolutions, some as fine as <10 m. The relatively coarse resolutions of common multispectral sensors, such as Landsat (30 m), have use for regional land cover mapping but are limited in observing localized vegetation change and the detailed fractionation of peatland cover type. Unlike SAR, multispectral sensors are only sensitive to spectral and thermal properties of the land-surface (often vegetation), but provide no direct information on vegetation geometry, vegetation water content, surface structure, or soil moisture.

Research has been conducted on the application of SAR for mapping distinct aspects of peatlands, with examples including: the monitoring of surface soil moisture conditions [23], [24], seasonal inundation patterns [25], and estimating properties of vegetation biomass [26], [27]. Much of the research conducted using SAR has focused on multipolarization datasets. These studies have provided knowledge on the most applicable frequencies and polarizations for application to detecting peatland properties, indicating that this depends on factors including the local wetland type, water level, vegetation structure, density, and height. For example, Baghdadi et al. [18] used C-band SAR for mapping wetland type in the Mer Bleue region near Ottawa, Canada, and demonstrated that $\sigma°HV$ was optimal for differentiating wetlands (forested and nonforested peat bogs) from other land covers, achieving a 76% overall pixel classification accuracy. At the same peatland site, Li and Chen [28] tested the fusion of optical, SAR, and digital elevation model (DEM) datasets for identifying open bog, open fen, treed bog, marsh, and swamp wetlands and reported overall classification accuracies of 71–92%. Whitcomb et al. [22] used L-band SAR imagery for mapping vegetated wetlands of Alaska and produced a high-resolution large-scale thematic map with 89% overall accuracy. Atwood et al. [29] also used L-band SAR to demonstrate an improved gamma naught ($\gamma°$) radiometric correction technique, through classification of a site within interior Alaska characterized by wetlands, herbaceous tundra, and evergreen and deciduous forests. With the application of this technique, woody wetlands were classified with 64% user's accuracy and 72% producer's accuracy.

Supplementary SAR information such as polarimetric decomposition parameters and image textures is also beneficial for assisting in wetland classifications. Incoherent decompositions, which express the average scattering mechanism of a distributed target (e.g., [30]–[32]), have become a widely researched technique for land cover classifications with SAR data, including wetlands. Two of the most commonly reported scattering decompositions are those of Cloude and Pottier [30] and Freeman and Durden [31]. Brisco et al. [33] found the Freeman–Durden decomposition effective at delineating wetland boundaries because of the characterization of double-bounce scattering from flooded vegetation. These researchers also found the Cloude–Pottier decomposition capable of classifying different plant functional groups within wetlands (65% overall accuracy). Antropov et al. [34] also used the Freeman–Durden scattering components to map soil types under vegetated peatlands with promising results (up to 70% overall accuracy). Walfir et al. [35] used manual interpretation techniques of RADARSAT-1 textures and tones for identifying wetland cover classes of the Brazilian Amazon. An accuracy assessment was not completed; however, they did conclude that the SAR texture products were fundamental in providing consistent wetland information. In another example, Arzandeh and Wang [36] used texture analysis to improve single-date radar images of a wetland complex and found that optimal multiple-texture combinations significantly improved the discrimination between wetland and nonwetland areas (88% overall accuracy classifications of wetlands vs. nonwetlands). The previously cited study by Whitcomb et al. [22] also used summer and winter JERS image texture (and other inputs and ancillary data), generated from the full-resolution (12.5 m) SAR backscatter, to assist in developing wetland classifications of Alaska.

Although various studies have explored the utility of SAR for peatland mapping, few have identified the combined influence of various SAR datasets at multiple incidence angles. Dual- or multi-angle approaches have shown to improve target characterization within other realms of SAR research (e.g., [37], [38]), thus justifying the need to explore this technique more thoroughly with a focus on wetland classification. Addressing this gap within the SAR literature may ultimately present an improved methodology for users applying SAR imaging in wetland-dominated environment. The objective of this paper is to assess the contributions of multipolarization backscatter, image textures, and two polarimetric SAR decompositions developed from the summer acquired RADARSAT-2 imagery for classifying subarctic boreal peatlands in the southern margin of discontinuous permafrost in northwestern Canada. The purpose of this research is to identify the importance of the Cloude–Pottier decomposition, Freeman–Durden decomposition, and various image textures to image classification, in contrast to backscatter information available only from multipolarization datasets. Additionally, we examine the impact of single image compared to combined dual-angle (two-image) image acquisitions on classification accuracies.

II. STUDY SITE AND TARGET LAND CLASSES

Research was conducted within the lower Liard River valley, in the Scotty Creek basin (Lower Liard watershed), Northwest Territories, Canada (see Fig. 1). Scotty Creek (61°18'N; 121°18'W) is a relatively small watershed (152 km^2) located 50 km south of Fort Simpson. Scotty Creek has a low drainage density (0.016 km km^{-2}) and basin slope (0.0032°) with
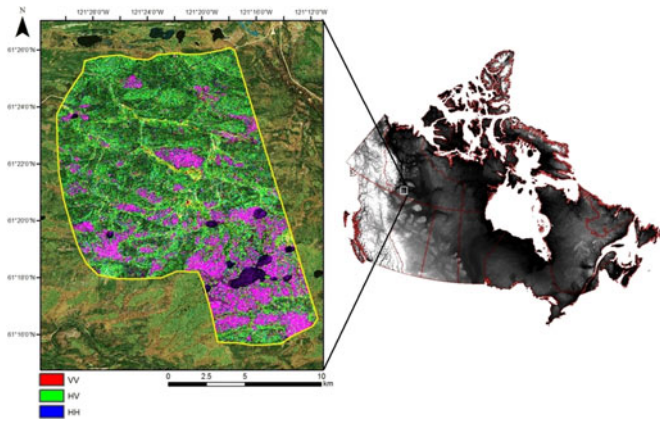
Fig. 1.   Location of the Scotty creek watershed, Northwest Territories, Canada.

elevation ranging between 240 and 290 m [39]. Scotty Creek watershed is located in the continental high boreal wetland region of Canada and within the DPZ. It is also within the Taiga Plains, a terrestrial ecozone consisting largely of coniferous forest with pines (Pinus), spruces (Picea), and larches (Larix), as well as aspens (Populus) and birches (Betula).

Scotty Creek watershed is a wetland-dominated landscape primarily consisting of peat plateaus, channel fens, flat bogs, wooded uplands, and open-surface water (see Fig. 2). These land cover types were of interest for the classifications performed in this study. Peat plateaus are underlain by a perennially frozen core [40] and rise 1–2 m above the regional water table due to the expansion of their frozen peat. Plateaus are forested (>70% tree cover) to wooded (30–70% tree cover), typically with a uniform cover of open-canopied black spruce (*Picea mariana*) [41]. Plateau ground cover contains various lichens and mosses, but is predominately ericaceous shrub and Sphagnum-dominated. Adjacent to plateaus are permafrost free flat bog and channel fen wetlands. This proximity supports the lateral exchange of runoff from raised plateaus to wetlands, while saturated wetland conditions have thermal influences on plateau edge degradation; these are unique hydrological processes of this ecosystem [39]. Channel fens are characteristically located along the drainage network of basins in the form of 50 to >100 m wide channels [11]. As a result, interconnected channel fens provide drainage pathways between major water bodies, such as lakes, through lateral flow conveyance [39]. Ombrotrophic flat bogs are featureless surfaces that form in broadly defined and poorly drained depressions. Sphagnum species mostly cover their featureless surfaces, which overlies yellowish peat with Sphagnum remains. Also prevalent are club-moss (Lycopodium), liverwort species (Marchantia), and various fungi [42]. The water table is at or slightly below the surface of bogs and they characteristically have low inputs of basic cations and nutrients, resulting in low pH (<4.5) [43]. This is contrasting to minerotrophic channel fens, which are commonly of neutral pH (>5.5) [43] because of their sources of groundwater which typically result in them being species-rich. Depending on their nutritional characteristics (e.g., fens can be classified as poor, moderate, or rich), fens may support a variety of brown mosses, trees, shrubs, sedges, or Sphagnum [14], [45], and thus their concentrations of biomass and vegetation are variable. Wooded uplands are located on well-

drained moraine deposits with rocky mineral soils that support tall deciduous-dominated mixed forests. As a result, vegetation foliage cover is generally greater than treed land covers found in the lower portions of the watershed (e.g., peat plateaus). Upland tree species predominately include a dense coverage of trembling aspen (*Populus tremuloides*), white spruce (*Picea glauca*), Alaskan birch (*Betula neoalaskana*), and jack pine (*Pinus banksiana*).

III.   METHODS

A.   RADARSAT-2 Imagery

For this study, four 25 km × 25 km C-band RADARSAT-2 SAR scenes (see Table I) were acquired over the Scotty Creek watershed. Two scenes were acquired in the summer of 2012 (July 22 and 31) and two in the summer of 2013 (August 26 and 27). All scenes were acquired in a RADARSAT-2 fine-quad (FQ) polarimetric beam mode at varying incidence angles (∼19°, 23°, 48°, and 46°) and in a single look complex format. All FQ scenes were illuminated in an ascending (right-looking) satellite orbit with 5.2 m × 7.6 m (range × azimuth) resolution. In this paper, RADARSAT-2 scenes will be referred to based on their beam mode acquisition (as shown in Table I).

1)   Polarimetric SAR Data Processing: All RADARSAT-2 images were preprocessed using PCI Geomatica 2013 software (see Fig. 3). POLSAR datasets were first ingested into the software (in PCIDSK format) and then filtered with a 5 × 5 low-pass mean (boxcar) filter to suppress speckle noise and to increase the effective number of looks of the single-look SAR data to 25. The boxcar filter algorithm preserves polarimetric information and operates in the spatial domain by replacing the center pixel in a moving window with the average of pixels in the assigned window size.

Filtered SAR images were then prepared for polarimetric dataset extraction by first converting to an appropriate matrix format. The symmetrized covariance (C3) matrix was used for extracting the HH, HV, and VV linear intensity channels, where H refers to horizontally polarized and V refers to vertically polarized. The VH linear intensity channel was not extracted, as the reciprocity theorem states that the information supplied by the HV channel is identical to VH. Pixel values of the linear intensity images also underwent radiometric calibration to produce dB values of sigma nought ($\sigma°$) using the equation:

$$\sigma° \,(\text{dB}) = 10\log_{10}\left(\sigma°_{\text{linear}}\right). \qquad (1)$$

Polarimetric decompositions were then applied to the filtered SAR imagery for identifying dominant backscattering mechanisms of peatland types and for the extraction of meaningful decomposition parameters. This research explored the Freeman–Durden [31] and Cloude–Pottier [30] decomposition methods, two of the most frequently applied methods for land cover interpretation (e.g., [33], [46]–[49]). The Freeman–Durden decomposition was used to partition the backscattering for each image pixel from the C3 matrix into the following scattering mechanisms: 1) double-bounce scattering, 2) volume scattering, and 3) rough-surface scattering. The Cloude–Pottier decomposition was then used to extract the entropy (*H*), anisotropy (*A*), and alpha angle (α) parameters from the symmetrized coherency (T3)

Target Class	Permafrost	Description	Ground Photo	Overhead Photo
Bog	Absent	Flat, featureless, *Sphagnum* dominated surface with a water table close to the surface. Sparse ericaceous shrubs, graminoids, and small forbs are often present.		
Fen	Absent	Broad channels with a thick floating vegetation mat. These features often have sparse cover or *Larix laricina* trees or *Betula* shrubs and have a diverse collection of non-vascular plants, graminoids, and forbs.		
Plateau	Present	Raised peat surface with a relatively open *Picea mariana* canopy. Ground surface is covered with *Sphagnum* and feather mosses and lichen with a layer of ericaceous shrubs and forbs.		
Upland	Present	Well-drained mineral deposits with a closed canopy forest comprised largely of *Populus tremuloides* and *Picea glauca*.		
Water	Absent	Open surface water bodies such as lakes.		

Fig. 2. General descriptions and photographs of Scotty Creek land covers.

TABLE I
RADARSAT-2 IMAGERY DETAILS

Acquisition Date	Polarization	Beam Mode	Central Inc. Angle	Orbit
22/07/2012	HH, HV, VH, VV	FQ1	19.4°	Ascending
31/07/2012	HH, HV, VH, VV	FQ30	48.1°	Ascending
26/08/2013	HH, HV, VH, VV	FQ27	45.8°	Ascending
27/08/2013	HH, HV, VH, VV	FQ4	23.1°	Ascending

matrix. H characterizes the amount of mixing between scattering mechanisms (eigen values), with single scattering mechanisms associated with values close to 0, and equal scattering mixes associated with values close to 1. A characterizes the amount of mixing between the second and third scattering mechanisms, where a value of 0 indicates equal proportions, and values close to 1 indicate that the second mechanism dominates. α ranges from 0° to 90°, with low values ($<40°$) representing surface scattering, intermediate (40° to 52.5°) representing double bounce, and high ($>52.5°$) values indicating volume scattering. A is most meaningful for low values of H. When H is close to 0, A values of 0° denote single-surface scattering, values of 45° refer to volume (dipole) scattering, and values of 90° indicate double-bounce scattering.
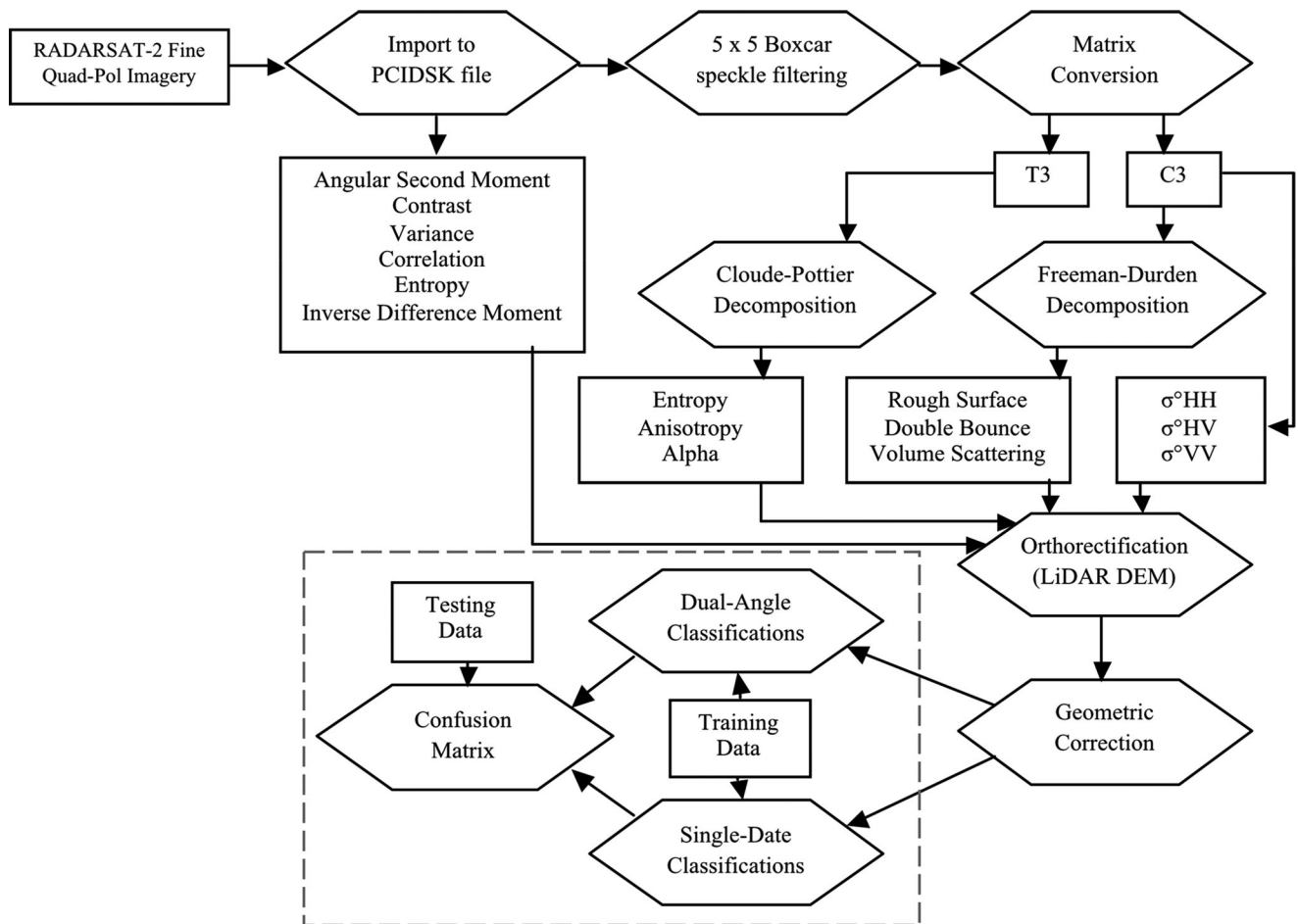
Fig. 3. Flowchart of polarimetric SAR processing for peatland classification.

In addition to linear intensities and polarimetric decomposition parameters, image texture information was also extracted for all pixels within each unfiltered RADARSAT-2 FQ image. Unfiltered images were used because of concerns with the loss of textural information from the application of SAR image filters [36]. Texture values were extracted from the total power (TP) of the SAR signal. The TP of an SAR image equals the span (i.e., sum) of the C3 matrix. Image texture describes the spatial arrangement and variation of patterns among image pixels within an image, and has shown to improve land cover classifications in wetland environment [50]–[52]. It, therefore, provides quantitative properties of smoothness, coarseness, and regularity of image pixels. The texture measures for this study were based on second-order statistics computed from the grey level co-occurrence matrices (GLCM). The GLCM can be defined as a tabulation of how often different combinations of pixel values (grey levels) occur throughout an image. Haralick *et al.* [53] introduced 14 statistical parameters that quantify image texture; however, the literature indicates six as being most relevant: angular second moment, contrast, variance, correlation, entropy, and inverse difference moment [52]. Therefore, these texture parameters were tested for image classification improvement. Texture values were extracted at a 5×5 pixel window, consistent with the filtering window applied to SAR imagery.

All extracted SAR datasets from the RADARSAT-2 FQ images were then orthorectified to provide terrain correction, due to varying projection between image and ground coordinates. The orthorectification process was completed with the PCI Geomatica 2013 Orthoengine extension. Images were corrected to a 2 m resolution airborne LiDAR DEM, collected by Hopkinson *et al.* [55], and using the bilinear interpolation resampling method, which incorporates the values of the four nearest input cell centers to determine the final value on the output raster. The MDA supplied rational function math model was also used for orthorectification, rather than manually collected ground control points. The extension's rational functions math model builds a correlation between an image's pixels and their ground locations. Images were then processed (geocoded) to UTM NAD 1983 with a postprocessing cell resolution of ~8 m.

B. Supervised Peatland Classifications

Linear intensities, decomposition parameters, and image textures were evaluated first in isolation (see Fig. 4) and then in combination to assess their contributions to peatland type identification. Lastly, datasets from large and small incidence angle imagery were combined for testing a dual-angular classification
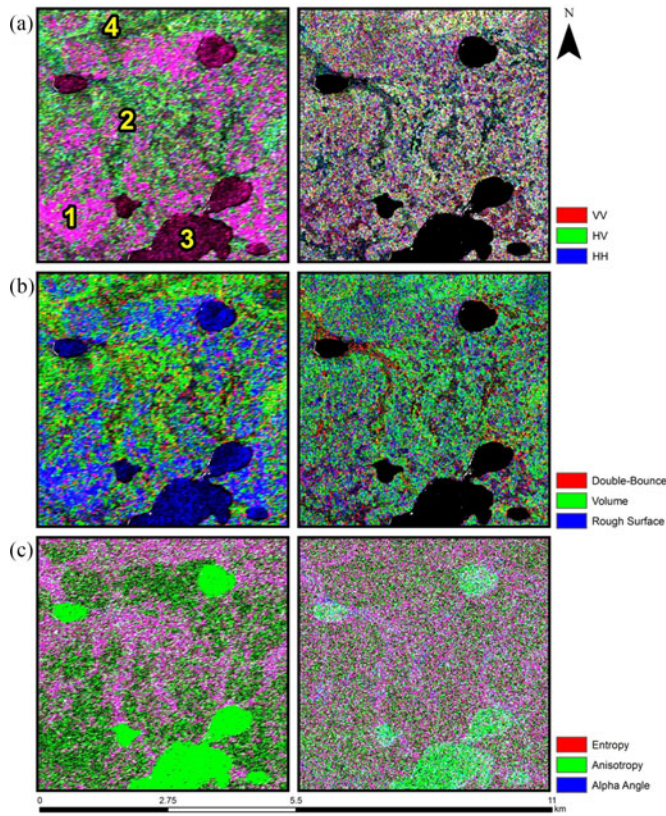
Fig. 4. Composites of SAR datasets at low and high incidence angles. (a) Linear intensities with small (left) and large (right) angle scenes, (b) Freeman–Durden parameters with small (left) and large (right) angle scenes, and (c) Cloude–Potter parameters with small (left) and large (right) angle scenes. Numbers indicate (1) bogs, (2) fen, (3) open water, and (4) uplands.

approach. The low temporal differences between images permitted this assessment, as the FQ1 and FQ30 scenes were captured nine days apart, and the FQ4 and FQ27 scenes were captured one day apart. All classifications required the development and input of multiband files, which were dependent on the assessment being completed. Multiband rasters were created with Exelis ENVI 4.8 software using the layer stacking toolbox.

To complete classifications, a support vector machine (SVM) supervised classifier (Exelis ENVI 4.8 software) was selected. First described by Vapnik [56], SVM classifiers are a supervised nonparametric statistical learning technique that operates by finding a hyperplane that separates the remotely sensed data into a predefined number of classes. The hyperplane is defined as the decision boundary that minimizes misclassifications based on the optimal separation of data within the feature space. Fundamental to the optimal hyperplane technique are the support vectors. Support vectors are the data points closest to the hyperplane that lie on the margin boundaries and are critical elements of the training set [57].

A Gaussian radial basis function kernel algorithm for the SVM was chosen because it has shown to handle more complex nonlinear class distributions, and is defined by the following equation:

$$K(x, y) = \exp(-y\|x - y\|^2) \quad (2)$$

TABLE II
NUMBER OF PIXELS USED FOR TRAINING AND TESTING

Target Class	Training Pixels	Testing Pixels
Bog	1339	1313
Fen	1344	1309
Plateau	1416	1241
Upland	1269	1468
Water	1350	1361

where $K(x, y)$ defines the kernel, x and y are the data being separated, and γ is the gamma parameter. The γ parameter defines how strong a single training example (i.e., one digitized target) influences the classification process, and is therefore the width of the kernel function. γ values for each image classification were the inverse of the number of bands (datasets) in the input image stack.

1) Training and Testing Data: Digitized polygon boundaries of peatland types used for training and testing were predominantly chosen based on highly accurate classification maps of Scotty Creek developed by Chasmer *et al*. [58], as well as GPS (Garmin eTrex) collected spatial information from overhead (Cessna 206 aircraft) and field surveys completed in August 2012 and May 2013. The Chasmer *et al*. [58] land cover maps were developed using a decision-tree classification approach from the fusion of airborne LiDAR and high-resolution WorldView-2 multispectral imagery. Chasmer *et al*. [58] used topographic derivatives and vegetation structural and spectral characteristics to produce classification accuracies between 88% and 97%, depending on land cover type. These accuracies were obtained by comparing with field surveyed (differential GPS) waterline extent of land covers.

Based on the described datasets, training and testing polygons were carefully digitized for SAR images for forested uplands, peat plateaus, flat bogs, channel fens, and open-surface water using ArcMap (ESRI ArcMap 10.1). Digitized targets were applied with an inward buffer of ~8 m (1 postprocessed RADARSAT-2 SAR pixel) or greater (dependent on image interpretation) to account for mixed pixel edges. This was also done to reduce speckle-related fluctuations in the backscattered data. Digitized polygon targets were randomly split (50:50) for the training and testing of supervised SVM classifications (see Table II). Testing sites used to validate SAR classifications were converted to regions of interest (ROI) in ENVI for developing confusion matrices—confusion matrices allow for visualization of a classifications performance by summarizing the relationship between two sources of information: 1) the classified image (i.e., the predicted class), and 2) ground-truthed data (i.e., the actual class). The confusion matrix tool in ENVI pairs ROIs with the land classes of a classification to show the percentage of ROI pixels that were or were not contained in a resulting class. Statistical assessments derived from the confusion matrices included the following: overall image classification accuracy (correctly classified pixels/total number of pixels), kappa coefficient (a measure between actual agreement and agreement by chance) producer's accuracy (correctly classified pixels for a given class/total number of pixels for that class as indicated

TABLE III
FIELD SURVEYED 0–5 CM DEPTH VOLUMETRIC SOIL MOISTURE (%)
COINCIDENT WITH SATELLITE OVERPASSES

Sampling Date	Overpass Beam Mode	Plateau Average Soil Moisture	Bog Average Soil Moisture	Fen Average Soil Moisture
22/07/2012	FQ1	9.74	80.63	70.27
31/07/2012	FQ30	12.30	69.79	52.07
26/08/2013	FQ27	15.15	79.78	67.32
27/08/2013	FQ4	26.46	84.43	79.78

Note: 156 measurements were taken on each date.

from the digitized ground-truthed reference data), and user's accuracy (correctly classified pixels for a given class/all pixels classified as that class) [59]. Producer's accuracy quantifies how well a certain area can be classified (omission error), whereas user's accuracy quantifies the reliability of classes in the classified image (commission error).

2) In Situ Soil Moisture Measurements: Soil moisture measurements at 0–5 cm depth were also acquired coincident with RADARSAT-2 overpasses. Satellite-based SAR backscatter can be related to surface moisture due to the contrast of dielectric constants of wet and dry surfaces [60], [61], making SAR ideal for observing hydrologic patterns in wetland environment. Therefore, soil moisture measurements assisted in the analysis and interpretation of classification results. Field measurements were conducted with Stevens Hydra Probe (Stevens Water Monitoring Systems, Inc.) and ML2x Delta-T Theta Probe (Delta-T Devices, Inc.) sensors and calibrated to <0.05 RMSE using oven-dying techniques. A total of 156 surface measurements were taken for each SAR overpass within a 140 m $\times$ 500 m sampling grid (20 m spacing) that spanned open bogs, channel fens, and permafrost plateaus. Table III presents the average field measured volumetric soil moisture for coincident overpasses by landcover class. Note that the wetland (bog and fen) measurements were often near saturation, a result of the water table being sufficiently close to the ground surface throughout most of the year, which satisfies the definition of "wetland" [62]. Additionally, high water tables within sampled wetlands remove the concern around the SAR signal penetrating deeper than 5 cm (the depth of the soil moisture sampling probe) in organic soils with high porosity, as the signal response is largely controlled by the dielectric from the (mostly) saturated conditions. Peat characteristics of plateaus, in contrast, typically have higher bulk density, and therefore this concern is reduced amongst these land covers with C-band SAR penetration.

IV. RESULTS AND DISCUSSION

A. Classifications Using Linear Intensities

Linear intensity channels (σ°HH $+ \sigma^\circ$HV $+ \sigma^\circ$VV) were first tested in isolation for target identification using each FQ RADARSAT-2 image. Results indicated that operationally suitable wetland classification accuracies ($>70\%$) can be achieved with a multipolarization SAR sensor in this peatland environment, however obtaining this result is beam mode dependent

as several classifications were $<70\%$ overall accuracy (see Table IV). When using linear intensities only, the small angle FQ1 image achieves the highest overall accuracy of 77% (0.71 kappa coefficient). This result supports previous studies indicating that small incidence angle SAR images ($<31°$) are optimal for boreal wetland mapping [63]. This in part because SAR sensors operating at small incidence angles better penetrate short shrub wetland vegetation found in bogs and fens, whereas observation at large incidence angles results in increased canopy attenuation and scattering due to the viewing geometry. This produces a backscattering response more similar to upland or plateau targets. However, while small angle SAR images were found to produce better results than large angle SAR images, the fact that the FQ1 linear intensity classification outperformed the FQ4 image by 9% suggests that factors other than the minimal difference in the incidence angle influenced the identification ability. To account for this, surface soil moisture measurements acquired during field sampling campaigns coincident with RADARSAT-2 overpasses were used to assist in the interpretation of the radar response. Surface conditions during the FQ4 acquisition were found to be vastly wetter over nonwetland land cover types (26% volumetric soil moisture) than during the FQ1 acquisition (10% volumetric soil moisture), and moisture measurements across fens and bogs were also drier for the FQ1 image acquisition. We hypothesize that contrasting dielectric between mostly saturated wetland surfaces and drier plateaus and uplands enhanced target separation for the FQ1 image. Therefore, although the contrast in results could be attributed to the variation in image beam modes, it is important to consider dynamic surface conditions and incorporate ancillary information (e.g., precipitation data) when available to assist in the interpretation of classification results.

When using only linear intensities, wetland classes were best identified with small angle imagery. Bogs were best classified with the FQ1 image, achieving a 95% producer's accuracy, whereas fens were best classified with the FQ4 image, achieving a 74% producer's accuracy (see Table IV). Bogs were easily identifiable with the FQ1 image, likely because of the high σ°HH backscatter from a combination of wet and rough peat surface conditions, which is very distinguishable in Fig. 4(a). However, classifications using only linear intensities produced poor differentiation between forested uplands and peat plateaus, indicating that C-band wavelength SAR had difficulty in discerning coniferous and deciduous components such as leafs, branches, and stems. Nevertheless, the FQ1 SAR image was able to classify peat plateaus with 81% producer's accuracy. This indicates that C-band SAR can, to some degree depending on beam mode selection, discriminate scattering events of plateaus and their typically black spruce (*P. mariana*) dominated surfaces from deciduous covered uplands. Open-surface water was identified with 100% producer's accuracies with all beam modes.

Linear backscatter intensity classification results are comparable to other studies, further supporting for the use of C-band SAR sensors over boreal peatland dominated environment. Li *et al.* [63] achieved classification producer's accuracies of ~80–86% for open and treed peatland bogs; however, their procedure included the addition of multispectral imagery and

TABLE IV
OVERALL CLASSIFICATION ACCURACIES (%) AND KAPPA COEFFICIENTS ($\hat{K}$) REPORTED FOR EACH SAR IMAGE, USING A SINGLE IMAGE APPROACH. PRODUCER'S ACCURACIES (%) FOR PEATLAND TYPES ARE ALSO REPORTED

Beam mode	Datasets	Bog	Fen	Plateau	Upland	Water	Overall Accuracy	$\hat{K}$
FQ1	Linear Intensities	95.8	65.3	81.1	46.2	100.0	77	0.71
	Freeman–Durden	96.8	63.9	81.8	36.9	100.0	75	0.69
	Cloude–Pottier	97.9	55.7	19.0	58.2	98.1	66	0.58
	Textures	68.1	21.8	53.5	13.1	32.1	37	0.22
	Linear + Freeman–Durden	96.5	63.3	81.4	48.8	100.0	77	0.72
	Linear + Cloude–Pottier	96.5	61.5	80.5	48.4	100.0	77	0.71
	Linear + Both Decompositions	96.7	61.7	79.2	46.8	100.0	76	0.70
	Linear + Textures	96.4	57.3	81.7	47.0	100.0	76	0.70
	Linear + Decompositions + Textures	96.8	57.8	82.1	47.5	100.0	76	0.70
FQ4	Linear Intensities	94.9	74.3	50.2	25.4	100.0	68	0.60
	Freeman–Durden	94.6	76.9	50.2	26.7	100.0	69	0.61
	Cloude–Pottier	90.7	22.1	53.6	59.3	98.1	65	0.56
	Textures	37.5	24.8	69.7	19.1	81.1	46	0.33
	Linear + Freeman–Durden	94.8	75.5	51.6	25.8	100.0	69	0.61
	Linear + Cloude–Pottier	95.6	76.7	51.7	30.7	100.0	70	0.63
	Linear + Both Decompositions	95.5	77.4	50.8	32.2	100.0	71	0.63
	Linear + Textures	94.9	77.2	53.1	25.9	100.0	70	0.62
	Linear + Decompositions + Textures	95.8	76.5	53.5	31.4	100.0	71	0.64
FQ27	Linear Intensities	68.6	54.3	66.1	36.1	100.0	65	0.56
	Freeman–Durden	71.4	60.3	60.7	39.8	100.0	66	0.58
	Cloude–Pottier	53.1	28.8	44.3	0.0	78.2	40	0.26
	Textures	9.7	50.0	82.4	6.9	100.0	49	0.37
	Linear + Freeman–Durden	70.2	57.8	65.9	39.1	100.0	66	0.58
	Linear + Cloude–Pottier	67.4	61.1	64.6	41.0	100.0	66	0.58
	Linear + Both Decompositions	67.4	61.7	64.6	42.3	100.0	67	0.59
	Linear + Textures	69.7	51.1	62.8	39.3	100.0	64	0.56
	Linear + Decompositions + Textures	67.9	59.9	63.8	40.2	100.0	67	0.58
FQ30	Linear Intensities	62.5	62.4	63.3	17.3	100.0	60	0.51
	Freeman–Durden	60.6	69.6	62.8	20.1	100.0	62	0.53
	Cloude–Pottier	29.7	54.0	41.5	0.0	70.7	38	0.24
	Textures	14.9	41.9	54.0	21.0	100.0	46	0.33
	Linear + Freeman–Durden	62.9	67.3	64.9	21.2	100.0	63	0.53
	Linear + Cloude–Pottier	64.0	69.2	65.5	20.3	100.0	63	0.54
	Linear + Both Decompositions	64.1	70.5	65.3	20.1	100.0	63	0.54
	Linear + Textures	69.0	56.6	58.5	24.2	100.0	61	0.52
	Linear + Decompositions + Textures	68.2	63.0	63.7	22.4	100.0	63	0.54

elevation data. Baghdadi *et al.* [18] confirmed that multipolarizations are necessary for achieving optimal results with active microwave sensors by demonstrating unique sensitivities of each linear channel to peatland types. For instance, they found $\sigma°$HV most suitable for separating forested from nonforested targets, and $\sigma°$HH to be very sensitive to open wetlands due to moisture conditions. Their overall classification accuracies were 74% for $\sigma°$HH alone, 76% for $\sigma°$HV alone, and 59% for $\sigma°$VV alone. Santoro *et al.* [64] also found $\sigma°_{HV}$ to show strong contrast between mature forest stands and open areas such as clear-cuts in boreal Sweden. Morrissey and Livingston [65] classified a complex mosaic of forests, fens, and bogs amongst other land cover types, with C-band obtaining an overall accuracy of 89%.

B. Classifications Using Polarimetric Decompositions

The Freeman–Durden and Cloude–Pottier decompositions were used to decompose the fully polarimetric SAR data into their respective components. Decomposed components were then tested alone to determine their ability to identify peatland types. Interpretations of decomposition components and their respective scattering mechanisms assisted in classification

analysis. It was established that the Freeman–Durden decomposition performed better in this environment than the Cloude–Pottier decomposition, as the volume, double-bounce, and rough-surface scattering contributions could better distinguish peatland types.

Freeman–Durden decompositions demonstrated that a given target's dominant scattering contributions are quite dependent on the imaging incidence angle, and that these contributions are most clearly differentiated with small angle imagery (see Fig. 5). For example, bogs were differentiated very well from fens with the FQ1 scene, as they displayed relatively high quantities of rough-surface scattering (83%) and low quantities of volume scattering (15%), whereas fens were dominated by volume scattering (66%). However, fens did share overlapping scattering signatures with plateaus and uplands. This is a product of dense vegetation coverage found on uplands and plateaus, and mostly moderate coverage with fens; therefore, their rates of volume-scattering are relatively high regardless of illumination angle (>57%). As expected, the separation of plateaus from uplands was also difficult; however, small angle imagery did prove better than large angle imagery, albeit only marginally. The FQ4 beam mode, in particular, showed better differentiation
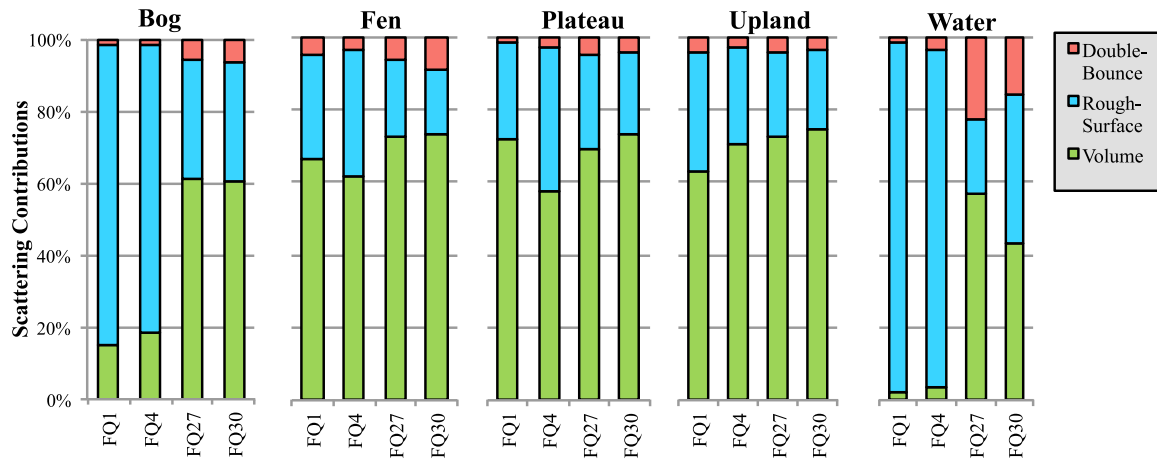
Fig. 5.   Freeman–Durden volume, double-bounce, and rough-surface scattering contributions of land cover targets.

of multiple-scattering events from these scenes, as uplands had 12% greater volume-scattering contributions than plateaus—it is possible that the moisture conditions during the time of the FQ4 image acquisition significantly influenced this result. Nevertheless, it is evident that physical geometric characteristics of vegetation stands found in upland environment (e.g., deciduous) and plateaus (e.g., coniferous) produces minor observable differences in scattering interactions regardless of the SAR imaging configuration. Although it must also be considered that the Freeman–Durden decomposition, like many other model-based decompositions, may be over estimating the volume scattering component of treed uplands and plateaus due to the occurrence of negative eigen values. The testing of other decompositions (e.g., [66], [67]) that account for this may improve results in this instance. Surface water targets were by and far the most contrasting land cover type. This is because surface water imparts minimal scattering from specular reflection, resulting in a very dark tonal upon visual inspection of the SAR image. Furthermore, any backscatter from water that was returned to the sensor could be attributed to Bragg scattering (a result of wind), although this was mostly absent due to open water targets being very calm.

Using the Cloude–Pottier decomposition, alpha-entropy feature space plots were developed for relating peatland types to physical scattering mechanisms (see Fig. 6). Alpha-entropy plots are divided into a series of separating boundaries referred to as sub–zones which assist in interpreting specific scattering characteristics of targets, as defined by Cloude and Pottier [30]. Similar to the Freeman–Durden decomposition, peatland types displayed more contrasting signatures with small angle SAR imagery.

With FQ1 and FQ4 images, bog targets existed primarily in zone 9, a product of low entropy ($H < 0.5$) and alpha angles ($<42°$). Targets that fall in this segmented zone characteristically exhibit single-scattering events such as surface scattering. Open-surface water targets also fell within this zone with small angle imagery because of specular surface scattering. Densely- and moderately-treed targets (e.g., uplands, plateaus, and fens) predominately fell in zones 5 and 6. Zone 5 indicates medium entropy vegetation scattering caused by a dominant double-bounce

(cylinder) type scattering mechanism whereas zone 6 reflects an increase in entropy caused by greater terrain surface roughness and due to canopy propagation effects [30]. Although plateaus and uplands mostly fell in zone 6, a number of sample targets also resided in zone 5. However, fen targets were mostly in zone 5, which is expected due to sparser vegetation cover. At large incidence angles, scattering signatures became extremely aggregated as all targets fell within zones 5 and 6. This degree of signature overlap was unexpected, especially for open-surface water targets that induce specular reflection. The conglomeration of targets with large angle images in the alpha-entropy zone-plots help explain the poor classification results at those respective incidence angles.

Following the analysis of decomposition parameters, the Freeman–Durden and Cloude–Pottier techniques were then tested for their contributions to classification potential. The FQ1 SAR image produced the best result with the Freeman–Durden decomposition, achieving a 75% overall accuracy (0.69 kappa coefficient) (see Table IV). Surface water was best identified with this beam mode and decomposition (100% producer's accuracy), followed by bogs (96.8% producer's accuracy) and plateaus (81.8% producer's accuracy). A greater degree of confusion was found with fen and upland targets (<64% producer's accuracies), as the decomposition indicated an overlap of scattering contributions. Regardless, this was a 9% overall improvement over the most successful classification using the Cloude–Pottier decomposition (66% overall accuracy with the FQ1 image). Comparable decomposition performances have been reported for wetland mapping [33]. We also established that for both decomposition techniques, accuracy was reduced as incidence angle became larger. Specifically, results demonstrated that the Cloude–Pottier decomposition parameters for both FQ27 and FQ30 images (<40% overall accuracy) resulted in confusion due to significant overlap of scattering properties among targets (see Fig. 6).

C. Classifications Using Image GLCM Textures

Image GLCM textures in isolation produced unsatisfactory peatland classifications (see Table IV). Classifications,
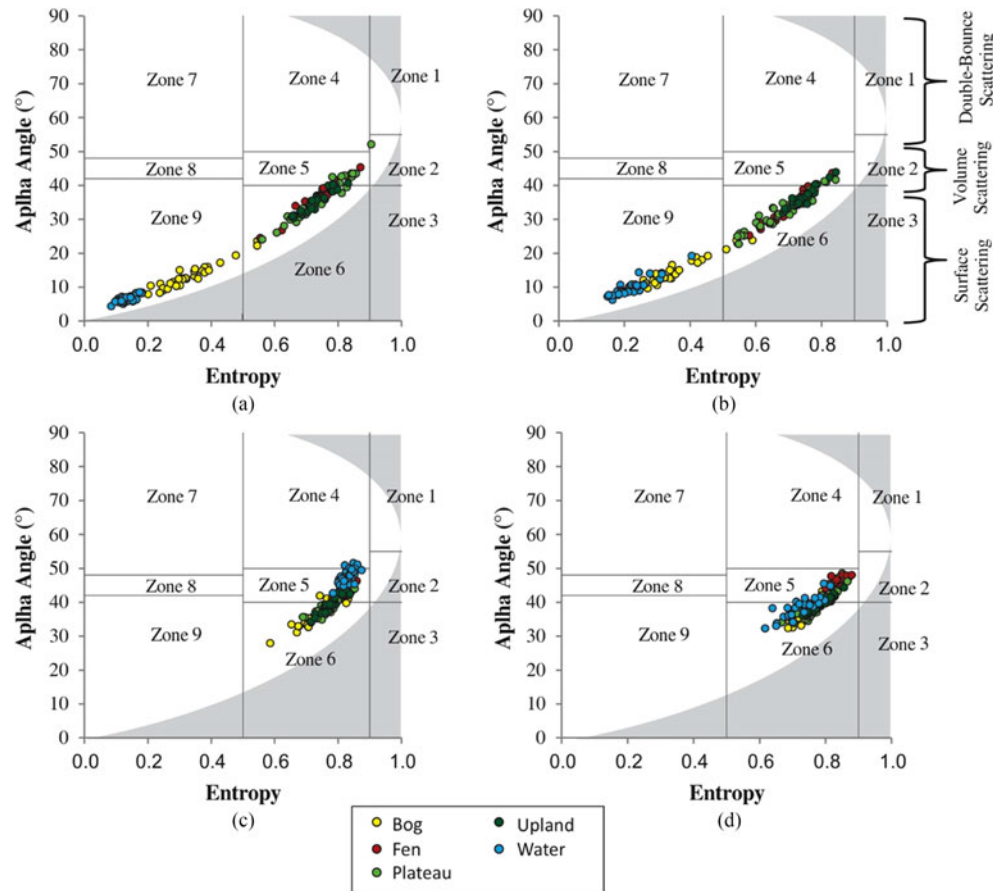
Fig. 6.   Cloude–Pottier entropy/alpha plots for study targets according to incidence angles of four RADARSAT-2 acquisitions in this study. (a) 19.4°, (b) 23.1°, (c) 45.8°, and (d) 48.1°. Zones are labeled according to [30].

regardless of beam mode, produced overall accuracies <50%. The FQ27 image produced the highest overall accuracy using image textures with a 49% overall accuracy (0.39 kappa coefficient). With small angle SAR images (FQ1 and FQ4), textures were the least successful SAR dataset in isolation, as overall accuracies were considerably lower than when using linear intensities or decompositions only. With large angle SAR images (FQ27 and FQ30), textures produced results only better than the Cloude–Pottier decomposition. Image textures were not as useful for identifying fen and upland targets, although modest success was found in classifying plateaus with large angle imagery (82% producer's accuracy with FQ27) and bogs with small angle imagery (68% producer's accuracy with FQ1). Success was achieved in surface water identification again though, as producer's accuracies of 100% were achieved with large angle FQ27 and FQ30 images. This is because water can be considered texture-less in SAR imagery due to little to no spatial variability, whereas in contrast, vegetated terrains represent a medium texture class [68].

It was hypothesized that a combination of image textures would produce better classification results in this environment, as previous research has shown SAR image textures to be valuable in wetland type identification [36], [52]. Arzandeh and Wang [36], in particular, were able to achieve 70% overall accuracy of their study site using SAR textures, as well as 80%

producer's accuracy for wetland types, a remarkably better result than in our study. However, to attain this result, their classification hierarchy approach was to simply differentiate wetland (e.g., marsh and swamp) from nonwetland terrain (e.g., urban, agriculture, etc.), a task that SAR is very capable of performing. They also experimentally tested various window sizes (from 3×3 to 25×25) for identifying an optimal texture dataset. As our study did not perform an exhaustive examination of window sizes, the potential for improving textural contributions to classification accuracy in this environment could be further explored. Racine et al. [69] also used SAR image textures in a peatland environment and classification results were more comparable to our results. They found that SAR textures (extracted using a 15/15 window) were able to achieve 36% overall accuracy for open peatland, forested peatland, water, and mineral targets. This in combination with the results from our study suggests that image textures derived from SAR imagery are not beneficial for peatland mapping, especially in subarctic boreal wetland dominated environment where interclass wetland differentiation is challenging.

D. Classifications Using Additively Combined SAR Datasets

Following the testing of unique SAR datasets in isolation, we then combined SAR datasets in an additive layer stacking approach for potentially improving peatland identification.

TABLE V
OVERALL CLASSIFICATION ACCURACIES (%) AND KAPPA COEFFICIENTS (K) USING A DUAL-ANGULAR APPROACH.
PRODUCER'S ACCURACIES (%) FOR PEATLAND TYPES ARE ALSO REPORTED

Beam modes	Datasets	Bog	Fen	Plateau	Upland	Water	Overall Accuracy	$\hat{K}$
FQ1	Linear Intensities	96.3	75.3	80.0	59.1	100.0	82	0.77
+	Freeman–Durden	97.1	79.8	82.1	56.4	100.0	83	0.78
FQ30	Cloude–Pottier	96.3	64.7	27.2	50.7	99.1	68	0.60
	Textures	72.3	34.9	66.7	23.9	99.5	59	0.49
	Linear + Freeman–Durden	96.8	76.3	80.9	63.5	100.0	83	0.79
	Linear + Cloude-Pottier	97.4	77.4	81.7	62.5	100.0	83	0.80
	Linear + Both Decompositions	97.4	77.9	81.3	63.2	100.0	84	0.80
	Linear + Textures	96.8	75.1	80.1	64.7	100.0	83	0.79
	Linear + Decompositions + Textures	97.1	76.7	80.2	68.4	100.0	84	0.80
FQ4	Linear Intensities	96.3	87.1	52.9	56.8	100.0	79	0.73
+	Freeman–Durden	93.4	85.2	51.7	54.3	100.0	77	0.71
FQ27	Cloude–Pottier	93.4	45.4	50.0	39.1	99.4	65	0.57
	Textures	56.9	44.9	58.7	25.6	100.0	57	0.46
	Linear + Freeman-Durden	96.5	87.7	56.9	57.7	100.0	80	0.75
	Linear + Cloude–Pottier	95.8	88.3	57.9	58.7	100.0	80	0.75
	Linear + Both Decompositions	96.0	88.6	57.8	59.4	100.0	80	0.75
	Linear + Textures	96.0	86.6	57.2	56.2	100.0	79	0.74
	Linear + Decompositions + Textures	96.1	87.3	61.4	56.4	100.0	81	0.76

Adding the Freeman–Durden or Cloude–Pottier decompositions to linear intensities produced ~1–3% overall accuracy improvements, apart from the FQ1 image in which no improvement was found (see Table IV). Combining both decompositions together with linear intensities also produced marginal improvements for most images, although a decrease in accuracy was found with the FQ1 image. It is understandable that little improvement was found with decompositions, as minimal double-bounce scattering was induced for all land covers. This suggests that there is not a dominant scattering mechanism for each class, thus assigning a classification based mostly on volume and surface scattering contributions is challenging. Overall accuracies were slightly reduced (~1%) with the FQ1 and FQ27 images when image textures were added to linear intensities, but improved when added to the FQ4 and FQ30 images (~1–3%). Results indicated that improvements were very modest for all dataset additions using single-date SAR imagery, though the best overall classification accuracies for the FQ4, FQ27, and FQ30 images (71%, 67%, and 63% overall accuracies) were achieved when stacking all linear intensity, decomposition, and texture information together. The FQ1 image was the only exception, as this beam mode found linear intensities only to produce a better overall classification (77% overall accuracy, 0.71 kappa coefficient) than with all collective datasets. Moreover, because overall classification improvements were minimal throughout the additive process, no particular land class had vastly enhanced identification results with added SAR datasets.

E. Classifications Using a Dual-Angular Approach

The dual-angular classification approach provided the most significant improvements in peatland type identification (see Table V). Several classifications achieved overall accuracies >80% using a combination of dual-angular imagery. Analogous to results observed with single-angular classifications, the Freeman–Durden decomposition outperformed the

Cloude–Pottier decomposition (>77% overall accuracies with Freeman–Durden components). Image textures performed poorly again (<59% overall accuracies), and generally produced little to no improvements as an additive dataset to linear intensities (~0–1% accuracy improvements). The highest overall accuracy (84% overall accuracy and 0.80 kappa coefficient) was achieved when combining all FQ1 and FQ30 linear intensities, polarimetric decomposition, and image texture datasets together [see Fig. 7(a)], although a similar result was achieved without image textures, further demonstrating that this information is unnecessary. This was a 7% overall accuracy improvement over the FQ1 linear intensity-only classification, which was the highest reported classification using only single-image datasets. Merging the FQ4 and FQ27 linear intensities, polarimetric decomposition, and image texture datasets also produced a strong classification of the Scotty Creek watershed for those respective dates, with a reported 81% overall accuracy and 0.79 kappa coefficient [see Fig. 7(b)].

Analysis of statistics generated from error matrices provides a valuable understanding of a classifier's performance. Full confusion matrices were generated for the two dual-angular classifications that utilized all SAR datasets, as these represent the best achievable results with their respective image combinations (see Tables VI and VII). Common trends of target identification and confusion were observed from the error matrices. First, both classifications indicated a very strong identification of bogs (>96% producer's accuracies), and less success with fens (>76% producer's accuracies). Fens were mostly misclassified as upland environment, suggesting that the rate of multiple scattering events from canopies and double-bounce scattering between trees and perpendicular surfaces causes confusion with upland targets when vegetation density is equivalent, or at least partially similar. Plateau and upland targets in particular were best identified with the FQ1 and FQ30 combined SAR datasets (80% and 68% producer's accuracies). Moreover, when these upland and plateau target classes were misclassified, they were
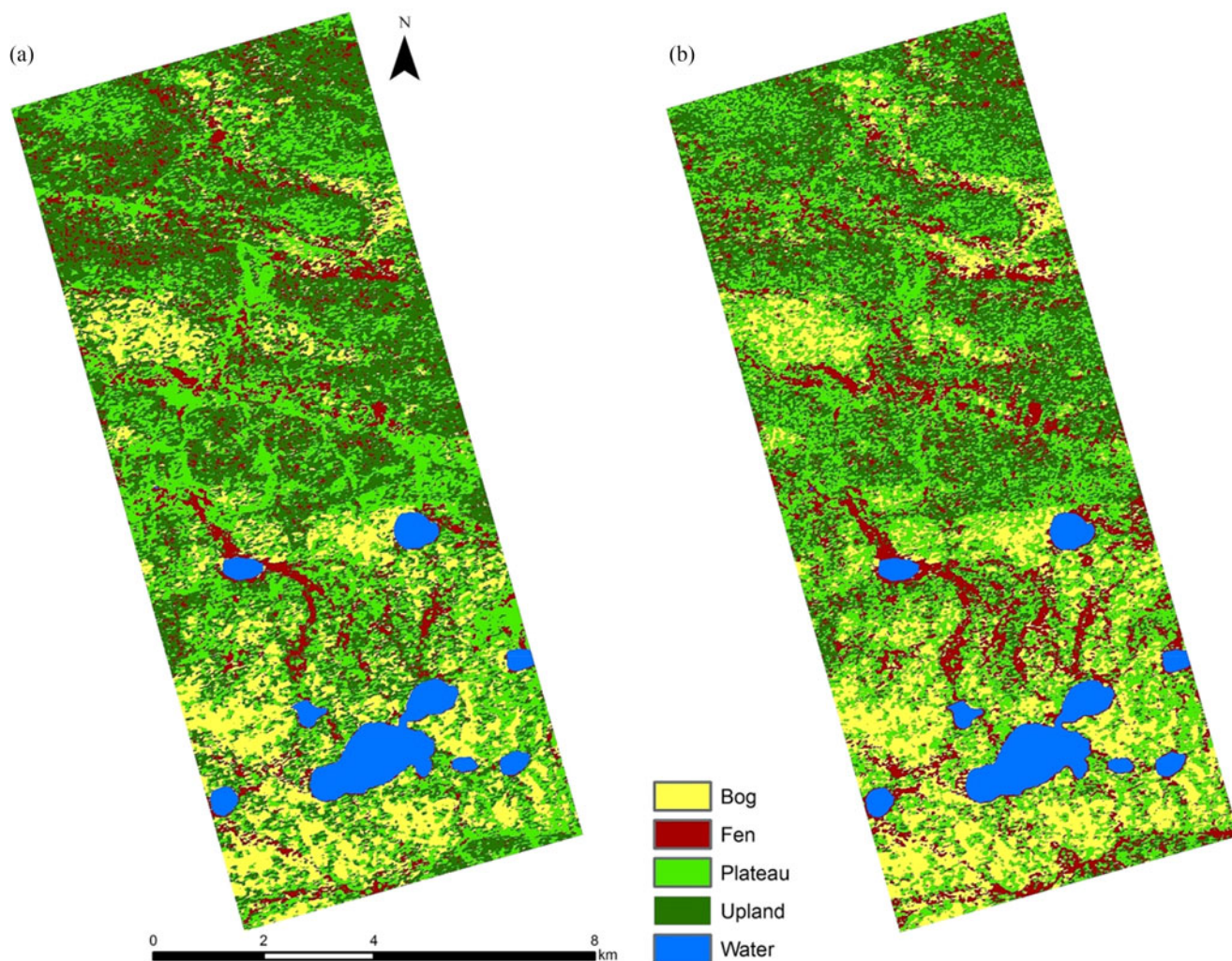
Fig. 7.   Image subsets of a high-density peatland region of Scotty Creek, classified using a dual-angular approach with linear intensity, decomposition, and texture datasets in combination. (a) FQ1 + FQ30 (84% overall accuracy, 0.80 kappa coefficient) and (b) FQ4 + FQ27 (81% overall accuracy, 0.79 kappa coefficient).

TABLE VI
CONFUSION MATRIX (NUMBER OF PIXELS) FOR THE FQ1 + FQ30
DUAL-ANGULAR CLASSIFICATION PERFORMED WITH LINEAR INTENSITY,
DECOMPOSITION, AND TEXTURE DATASETS COMBINED.
PRODUCER'S AND USER'S ACCURACIES ARE REPORTED IN %

		Reference Data					
		Bog	Fen	Plateau	Upland	Water	User's Ac.
	Bog	**1276**	12	9	19	0	96.9
	Fen	3	**1005**	3	158	0	85.9
Classified Image	**Plateau**	16	73	**996**	289	0	72.6
	Upland	18	219	233	**1005**	0	68.1
	Water	0	0	0	0	**1361**	100.0
	Producers Ac.	97.1	76.7	80.2	68.4	100.0	

Note: Overall accuracy = 84%, $\hat{K}$ = 0.76.

TABLE VII
CONFUSION MATRIX (NUMBER OF PIXELS) FOR THE FQ4 + FQ27
DUAL-ANGULAR CLASSIFICATION PERFORMED WITH LINEAR INTENSITY,
DECOMPOSITION, AND TEXTURE DATASETS COMBINED.
PRODUCER'S AND USER'S ACCURACIES ARE REPORTED IN %

		Reference Data					
		Bog	Fen	Plateau	Upland	Water	User's Ac.
	Bog	**1263**	18	67	0	0	93.6
	Fen	28	**1144**	48	182	0	81.6
Classified Image	**Plateau**	22	48	**763**	414	0	61.1
	Upland	0	99	363	**872**	0	65.3
	Water	0	0	0	0	**1361**	100.0
	Producers Ac.	96.1	87.3	61.4	59.4	100.0	

Note: Overall accuracy = 81%, $\hat{K}$ = 0.80.

predominately mistaken for each other. This again is due to comparable volume scattering events from canopy top-crown interactions, as revealed by decomposition components (see Fig. 5). This also indicates that additional frequencies (e.g., L- or P-bands) are likely necessary for improving forest stand differentiation, which is a contrasting notion to earlier work by Rignot *et al*. [70]. However, vegetation density must be considered if multiband frequencies are to be explored for this, as studies such as [71] have shown canopy penetrating L-band to be sensitive to surface moisture under 3 kg m^{-2} in black spruce (*P. mariana*) boreal forests.

The dual-angular approach with C-band SAR shows overall promising applications as a high-accuracy tool, specifically for the identification of saturated bogs, open water bodies, and forested terrains in permafrost environment. This can be extremely valuable for monitoring the following key issues: 1) the expansion of saturated bog terrain from permafrost thaw, and 2) the terrestrialization of open water bodies. In boreal environment such as Scotty Creek, research has revealed that horizontal heat flows in thawing discontinuous permafrost produce considerable land cover change [72]. This is vital at wetland–plateau interfaces, where plateaus are subject to rapid permafrost degradation and the subsequent conversion to saturated bogs. Using SAR to identify the spatial expansion of bogs can potentially be used to quantify areal extent of permafrost loss, in addition to assisting in understanding the organic matter accumulation and nutrient status of peatlands as permafrost continues to degrade [73]. Northern peatland environment is also beginning to show signs of open water terrestrialization as peatlands encroach lakes and ponds [74]. The capability to accurately delineate water bodies with a cost-effective method such as SAR lends to the potential for monitoring peat expansion under warming climatic conditions.

V. CONCLUSION

The cold and poorly drained conditions of northern boreal peatlands have resulted in the formation of thick soil carbon reservoirs that are highly sensitive to surface disturbances such as the thawing of permafrost. These reservoirs have the potential to alter global atmospheric greenhouse gas compositions and therefore have important implications on policy development and initiatives for combating climate change. Accurate monitoring and land cover change detection are necessary for understanding these disturbances and subsequent release of greenhouse gases from peatlands. Therefore, this research investigated the contributions of linear backscatter, two polarimetric decompositions, and image textures from polarimetric RADARSAT-2 SAR imagery for classification of a peatland-dominated subarctic environment.

This research provided an assessment of the contributions of linear backscatter compared to advanced polarimetric decompositions and image textures for peatland-type classification. Results demonstrated that when variables were assessed individually, multipolarized backscatter ($\sigma°$HH, $\sigma°$HV, $\sigma°$VV) generally produced comparable classification results to those of the Freeman–Durden and Cloude–Pottier decompositions regardless of the incidence angle. When combining additional polarimetric and texture datasets into classifications involving linear backscatter, the improvements were generally only minor. However, results also show that dual-angular classifications consistently outperform those of the single-angular approach. This is largely a result of combining complementary scattering information from small and large incidence angle imagery, thus becoming more sensitive to different peatland type properties. In general, target classification was most successful with the identification of isolated bogs and open water surfaces. Channel fens, uplands, and plateaus were commonly misclassified with each other to varying degrees, and the extent of misclassification depended on the SAR beam mode. Variations in environmental and weather conditions during SAR image acquisitions may also result in misclassification, as the sensitivity of C-band to heavy rain and wet conditions is well documented (e.g., [75]–[78]). The highest rate of misclassification was found with densely treed targets such as uplands and plateaus. However, since they were mostly mistaken for each other indicates that C-band SAR can accurately separate treed from nontreed terrain based on volume scattering contributions, but that confusion occurs when attempting to distinguish one treed target from another. This appears to be independent of biomass or tree species, as upland moraines are often deciduous or mixed forest whereas plateaus are commonly stands of mature black spruce (*P. mariana*). The application of multidate imagery spanning a large temporal period could improve this separation with leaf-on and leaf-off conditions [79]. The general confusion of tree type is less important for mapping permafrost extent in subarctic boreal Canada. For this reason, we concluded that C-band SAR is most applicable as a tool for monitoring change in permafrost boundaries and for terrestrialization of open water.

The implications of this research involve future sensor choice and testing for wetland classification, particularly as new C-band SAR sensors are available, such as RADARSAT-constellation mission (RCM) and Sentinel-1. The assessment of polarimetric contributions to image classification provides a unique assessment of the benefit of exploiting such complex SAR datasets for this application. It is suggested that future research over similar landscapes investigate the contributions of multiband SAR imagery for assisting in the separation of treed land covers such as uplands and plateaus from treed wetlands, as longer wavelengths (e.g., L-band) provide increased penetration of canopy structures. For example, previous studies such as [19] detail the need for L-band data for classification of fen types in high-latitude regions. Furthermore, exploration into the seasonal timing effects of image acquisition may yield worthy results, as leaf-off conditions from deciduous upland vegetation could assist in improving overall mapping accuracies at C-band. An assessment that combines imagery from varying hydrological states of the same sites is also of interest, as temporal differences have often been used to distinguish wetland types. Finally, further evaluation of the datasets and methodologies investigated in this research over other wetland-dominated basins in the subarctic should be explored.

REFERENCES

[1] E. Gorham, "Northern peatlands: Role in the carbon cycle and probable responses to climate warming," *Ecological Appl.*, vol. 1, no. 2, pp. 182–195, 1991.

[2] L. Chasmer, C. Hopkinson, and W. Quinton, "Quantifying errors in discontinuous permafrost plateau change from optical data, Northwest Territories, Canada: 1947–2008," *Can. J. Remote Sens.*, vol. 36, no. 2, pp. S211–S223, 2010.

[3] L. Chasmer, A. Kenward, W. L. Quinton, and R. Petrone, "CO_2 exchanges within zones of rapid conversion from permafrost plateau to bog and fen land cover types," *Arctic, Antarctic Alpine Res.*, vol. 44, no. 4, pp. 399–411, 2012.

[4] W. L. Quinton, M. Hayashi, and L. E. Chasmer, "Peatland hydrology of discontinuous permafrost in the Northwest Territories: Overview and synthesis," *Can. Water Resour. J.*, vol. 34, no. 4, pp. 311–328, 2009.

[5] V. E. Romanovsky, S. L. Smith, and H. H. Christiansen, "Permafrost thermal state in the polar northern hemisphere during the international polar year 2007–2009: A synthesis," *Permafrost Periglacial Process.*, vol. 21, pp. 106–116, Jun. 2010.

[6] S. D. Bridgham, J. P. Megonigal, J. K. Keller, N. B. Bliss, and C. Trettin, "The carbon balance of North American wetlands," *Wetlands*, vol. 26, no. 4, pp. 889–916, 2006.

[7] Q. Zhuang *et al.*, "CO_2 and CH_4 exchanges between land ecosystems and the atmosphere in northern high latitudes over the 21st century," *Geophys. Res. Lett.*, vol. 33, pp. 1–5, 2006, Art.ID. L17403.

[8] D. Beilman and S. Robinson, "Peatland permafrost thaw and landform type along a climatic gradient," in *Proc. 8th Int. Conf. Permafrost*, 2003, pp. 61–65.

[9] M. C. Serreze *et al.*, "Observational evidence of recent change in the northern high-latitude environment," *Clim. Change*, vol. 46, nos. 1–2, pp. 159–207, 2000.

[10] R. F. Connon, W. L. Quinton, J. R. Craig, and M. Hayashi, "Changing hydrologic connectivity due to permafrost thaw in the lower Liard River valley, NWT, Canada," *Hydrol. Process.*, vol. 28, no. 14, pp. 4163–4178, 2014.

[11] W. L. Quinton, M. Hayashi, and A. Pietroniro, "Connectivity and storage functions of channel fens and flat bogs in northern basins," *Hydrol. Process.*, vol. 17, pp. 3665–3684, Dec. 2003.

[12] N. Wright, M. Hayashi, and W. L. Quinton, "Spatial and temporal variations in active layer thawing and their implication on runoff generation in peat-covered permafrost terrain," *Water Resour. Res.*, vol. 45, pp. 1–13, May 2009, Art.ID. W05414.

[13] W. R. Rouse, "The energy and water balance of high-latitude wetlands: Controls and extrapolation," *Global Change Biol.*, vol. 6, no. Suppl. 1, pp. 59–68, Dec. 2000.

[14] C. Tarnocai, "The effect of climate change on carbon in Canadian peatlands," *Global Planet. Change*, vol. 53, pp. 222–232, 2006.

[15] M. Turetsky, R. Wieder, D. Vitt, R. Evans, and K. Scott, "The disappearance of relict permafrost in boreal north America: Effects on peatland carbon storage and fluxes," *Global Change Biol.*, vol. 13, pp. 1922–1934, Sep. 2007.

[16] K. Schaefer, T. Zhang, L. Bruhwiler, and A. Barrett, "Amount and timing of permafrost carbon release in response to climate warming," *Tellus*, vol. 63B, pp. 165–180, Apr. 2011.

[17] IPCC, "Climate Change 2014: Synthesis Report. Contribution of Working Groups I, II and III to the Fifth Assessment Report of the Intergovernmental Panel on Climate Change," IPCC, Geneva, Switzerland, Rep. no. ISBN 978-92-9169-143-2, 2014.

[18] N. Baghdadi, M. Bernier, R. Gauthier, and I. Neeson, "Evaluation of C-band SAR data for wetlands mapping," *Int. J. Remote Sens.*, vol. 22, no. 1, pp. 71–88, Jan. 2001.

[19] S. Durden, Z. Haddad, L. Morrissey, and G. Livingston, "Classification of radar imagery over boreal regions for methane exchange studies," *Int. J. Remote Sens.*, vol. 17, pp. 1267–1273, 1996.

[20] A. Lönnqvist, Y. Rauste, M. Molinier, and T. Häme, "Polarimetric SAR data in land cover mapping in boreal zone," *IEEE Trans. Geosci. Remote Sens.*, vol. 48, no. 10, pp. 3652–3662, Oct. 2010.

[21] J. Reschke, A. Bartsch, S. Schlaffer, and D. Schepaschenko, "Capability of C-band SAR for operational wetland monitoring at high latitudes," *Remote Sens.*, vol. 4, pp. 2923–2943, Oct. 2012.

[22] J. Whitcomb, M. Moghaddam, K. McDonald, J. Kellndorfer, and E. Podest, "Mapping vegetated wetlands of Alaska using L-band radar satellite imagery," *Can. J. Remote Sens.*, vol. 35, no. 1, pp. 54–72, Jun. 2009.

[23] A. Jacome, M. Bernier, K. Chokmani, Y. Gauthier, J. Poulin, and D. De Sève, "Monitoring volumetric surface soil moisture content at the La Grande basin boreal wetland by radar multi polarization data," *Remote Sens.*, vol. 5, pp. 4919–4941, Oct. 2013.

[24] E. S. Kasischke, L. L. Bourgeau-Chavez, and J. F. Johnstone, "Assessing spatial and temporal variations in surface soil moisture in fire-disturbed black spruce forests in Interior Alaska using spaceborne synthetic aperture radar imagery—Implications for post-fire tree recruitment," *Remote Sens. Environ.*, vol. 108, pp. 42–58, May 2007.

[25] A. Trofaier, A. Bartsch, W. Rees, and M. Leibman, "Assessment of spring floods and surface water extent over the Yamalo-Nenets autonomous district," *Environ. Res. Lett.*, vol. 8, 2013, Art.ID. 045026.

[26] Y. Rauste, "Multi-temporal JERS SAR data in boreal forest biomass mapping," *Remote Sens. Environ.*, vol. 97, pp. 263–275, Jul. 2005.

[27] M. Santoro, L. Eriksson, J. Askne, and C. Schmullius, "Assessment of stand-wise stem volume retrieval in boreal forest from JERS-1 L-band SAR backscatter," *Int. J. Remote Sens.*, vol. 27, no. 16, pp. 3425–3454, Aug. 2006.

[28] J. Li and W. Chen, "A rule-based method for mapping Canada's wetlands using optical, radar and DEM data," *Int. J. Remote Sens.*, vol. 26, no. 22, pp. 5051–5069, Nov. 2005.

[29] D. K. Atwood, D. Small, and R. Gens, "Improving PolSAR land cover classification with radiometric correction of the coherency matrix," *IEEE J. Sel. Topics Appl. Earth Observ. Remote Sens.*, vol. 5, no. 3, pp. 848–856, Jun. 2012.

[30] S. R. Cloude and E. Pottier, "An entropy based classification scheme for land applications of polarimetric SAR," *IEEE Trans. Geosci. Remote Sens.*, vol. 35, no. 1, pp. 68–78, Jan. 1997.

[31] A. Freeman and S. L. Durden, "A three-component scattering model for polarimetric SAR data," *IEEE Trans. Geosci. Remote Sens.*, vol. 36, no. 3, pp. 963–973, May 1998.

[32] R. Touzi, "Target scattering decomposition in terms of roll-invariant target parameters," *IEEE Trans. Geosci. Remote Sens.*, vol. 45, no. 1, pp. 73–84, Jan. 2007.

[33] B. Brisco, M. Kapfer, T. Hirose, B. Tedford, and J. Liu, "Evaluation of C-band polarization diversity and polarimetry for wetland mapping," *Can. J. Remote Sens.*, vol. 37, no. 1, pp. 82–92, Jun. 2011.

[34] O. Antropov, Y. Rauste, H. Astola, J. Praks, T. Hame, and M. Hallikainen, "Land cover and soil type mapping from spaceborne PolSAR data at L-band with probabilistic neural network," *IEEE Trans. Geosci. Remote Sens.*, vol. 52, no. 9, pp. 5256–5270, Sep. 2014.

[35] P. Walfir, M. S. Filho, and W. R. Paradella, "Use of RADARSAT-1 fine mode and Landsat-5 TM selective principal component analysis for geomorphological mapping in a macrotidal mangrove coast in the Amazon Region," *Can. J. Remote Sens.*, vol. 31, no. 3, pp. 214–224, Jun. 2005.

[36] S. Arzandeh and J. Wang, "Texture evaluation of RADARSAT imagery for wetland mapping," *Can. J. Remote Sens.*, vol. 28, no. 5, pp. 653–666, Jun. 2002.

[37] F. Dell'Acqua, P. Gamba, and G. Lisini, "Improvements to urban area characterization using multitemporal and multiangle SAR images," *IEEE Trans. Geosci. Remote Sens.*, vol. 41, no. 9, pp. 1996–2004, Sep. 2003.

[38] J. Shang, H. McNairn, J. Deschamps, and X. Jiao, "In-season crop inventory using multi-angle and multi-pass RADARSAT-2 SAR data over the Canadian prairies," *Proc. SPIE—Int. Soc. Opt. Eng.*, vol. 8156, 2011, Art.ID. 815604.

[39] M. Hayashi, W. L. Quinton, A. Pietroniro, and J. J. Gibson, "Hydrologic functions of wetlands in a discontinuous permafrost basin indicated by isotopic and chemical signatures," *J. Hydrol.*, vol. 296, pp. 81–97, Aug. 2004.

[40] S. Zoltai and C. Tarnocai, "Perennially frozen peatlands in the western arctic and subarctic of Canada," *Can. J. Earth Sci.*, vol. 12, pp. 28–43, 1975.

[41] L. Halsey and D. Vitt, "Disequilibrium response of permafrost in boreal continental western Canada to climate change," *Clim. Change*, vol. 30, pp. 57–73, 1995.

[42] S. Zoltai and D. Vitt, "Canadian wetlands: Environmental gradients and classification," *Vegetation*, vol. 118, pp. 131–137, 1995.

[43] S. D. Bridgham, K. Updegraff, and J. Pastor, "Carbon, nitrogen, and phosphorus mineralization in northern wetlands," *Ecology*, vol. 79, no. 5, pp. 1545–1561, 1998.

[44] M. Fafard, "Musical chairs in a boreal peatland: How permafrost that reverses successional processes," M.Sc. thesis, Wilfred Laurier Univ., Waterloo, ON, Canada, 2014.

[45] D. Vitt, L. Halsey, and S. Zoltai, "The bog landforms of continental western Canada in relation to climate and permafrost patterns," *Arctic Alpine Res.*, vol. 26, pp. 1–13, 1994.

[46] K. Li, B. Brisco, S. Yun, and R. Touzi, "Polarimetric decomposition with RADARSAT-2 for rice mapping and monitoring," *Can. J. Remote Sens.*, vol. 38, no. 2, pp. 169–179, Jun. 2012.

[47] B. Brisco, A. Schmitt, K. Murnaghan, S. Kaya, and A. Roth, "SAR polarimetric change detection for flooded vegetation," *Int. J. Digit. Earth*, vol. 6, no. 2, pp. 103–114, Mar. 2013.

[48] L. Sartori, N. Imai, J. Mura, E. Novo, and T. Silva, "Mapping macrophyte species in the Amazon floodplain wetlands using fully polarimetric ALOS/PALSAR data," *IEEE Trans. Geosci. Remote Sens.*, vol. 49, no. 12, pp. 4717–4728, Dec. 2011.

[49] C. Marechal, E. Pottier, L. Hubert-Moy, and S. Rapinel, "One year wetland survey investigations from quad-pol RADARSAT-2 time-series SAR images," *Can. J. Remote Sens.*, vol. 38, no. 3, pp. 240–252, Jun. 2012.

[50] Z. Szantoi, F. Escobedo, A. Abd-Elrahman, S. Smith, and L. Pearlstine, "Analyzing fine-scale wetland composition using high resolution imagery and texture features," *Int. J. Appl. Earth Observ. Geoinf.*, vol. 23, pp. 204–212, Aug. 2013.

[51] Z. Wentao, W. Bingfang, J. Hongbo, and L. Hua, "Texture classification of vegetation cover in high altitude wetlands zone," *Conf. Ser. Earth Environ. Sci.*, vol. 17, Mar. 2014, Art.ID. 012083.

[52] Y. Yamagata and Y. Yasuoka, "Classification of wetland vegetation by texture analysis methods using ERS-1 and JERS-1 images," in *Proc. Int. Geosci. Remote Sens. Symp.*, 1993, pp. 1614–1616.

[53] R. M. Haralick, K. Shanmugam, and I. Dinstein, "Textural features for image classification," *IEEE Trans. Syst. Man. Cybern.*, vol. 3, no. 6, pp. 610–621, Nov. 1973.

[54] R. Cossu, "Segmentation by means of textural analysis," *Pixel*, vol. 1, no. 2, pp. 21–24, 1988.

[55] C. Hopkinson *et al.*, "Moving toward consistent ALS monitoring of forest attributes across Canada," *Photogramm. Eng. Remote Sens.*, vol. 79, no. 2, pp. 159–173, 2013.

[56] V. Vapnik, *Estimation of Dependences Based on Empirical Data*. Moscow, Russia: Nauka, 1979, pp. 5165–5184.

[57] G. Mountrakis, J. Im, and C. Ogole, "Support vector machines in remote sensing: a review," *ISPRS J. Photogramm. Remote Sens.*, vol. 66, pp. 247–259, May 2011.

[58] L. Chasmer, C. Hopkinson, T. Veness, W. Quinton, and J. Baltzer, "A decision-tree classification for low-lying complex land cover types within the zone of discontinuous permafrost," *Remote Sens. Environ.*, vol. 143, pp. 73–84, Mar. 2014.

[59] R. G. Congalton, "A review of assessing the accuracy of classifications of remotely sensed data," *Remote Sens. Environ.*, vol. 37, pp. 35–46, 1991.

[60] F. Ulaby, P. Dubois, and J. van Zyl, "Radar mapping of surface soil moisture," *J. Hydrol.*, vol. 184, nos. 1–2, pp. 57–84, 1996.

[61] P. Dubois, J. van Zyl, and T. Engman, "Measuring soil moisture with imaging radars," *IEEE Trans. Geosci. Remote Sens.*, vol. 33, no. 4, pp. 915–926, Aug. 1995.

[62] N. W. W. Group, The Canadian Wetland Classification System, 2nd ed. Waterloo, ON, Canada: Wetlands Research Centre, 1997.

[63] J. Li, W. Chen, and R. Touzi, "Optimum RADARSAT-1 configurations for wetlands discrimination: A case study of the Mer Bleue peat bog," *Can. J. Remote Sens.*, vol. 33, no. 1, pp. S46–S55, 2007.

[64] M. Santoro, J. Fransson, L. Eriksson, and L. Ulander, "Clear-cut detection in Swedish boreal forest using multi-temporal ALOS PALSAR backscatter data," *IEEE J. Sel. Top. Appl. Earth Observ. Remote Sens.*, vol. 3, no. 4, pp. 618–631, Dec. 2010.

[65] L. Morrissey and G. Livingston, "Use of SAR in regional methane exchange studies," *Int. J. Remote Sens.*, vol. 15, no. 6, pp. 1337–1342, 1994.

[66] M. Arii, J. van Zyl, and Y. Kim, "Adaptive model-based decompostion of polarimetric SAR covariance matrices," *IEEE Trans. Geosci. Remote Sens.*, vol. 49, no. 3, pp. 1104–1113, Mar. 2011.

[67] Y. Yamaguchi, T. Moriyama, M. Ishido, and H. Yamada, "Four-component scattering model for polarimetric SAR image decomposition," *IEEE Trans. Geosci. Remote Sens.*, vol. 43, no. 8, pp. 1699–1706, Aug. 2005.

[68] F. Ulaby, F. Kouyate, B. Brisco, and T. Lee Williams, "Textural information in SAR images," *IEEE Trans. Geosci. Remote Sens.*, vol. GE-24, no. 2, pp. 235–245, Mar. 1986.

[69] M. Racine, M. Bernier, and T. Ouarda, "Evaluation of RADARSAT-1 images acquired in fine mode for the study of boreal peatlands: A case study in James Bay, Canada," *Can. J. Remote Sens.*, vol. 31, no. 6, pp. 450–467, Jun. 2014.

[70] E. J. M. Rignot, C. L. Williams, J. Way, and L. A. Viereck, "Mapping of forest types in Alaskan boreal forests using SAR imagery," *IEEE Trans. Geosci. Remote Sens.*, vol. 32, no. 5, pp. 1051–1059, Sep. 1994.

[71] L. Bourgeau-Chavez, B. Leblon, F. Charbonneau, and J. Buckley, "Evaluation of polarimetric Radarsat-2 SAR data for development of soil moisture retrieval algorithms over a chronosequence of black spruce boreal forests," *Remote Sens. Environ.*, vol. 132, no. 15, pp. 71–85, 2013.

[72] W. L. Quinton, M. Hayashi, and L. E. Chasmer, "Permafrost-thaw induced land-cover change in the Canadian subarctic: Implications for water resources," *Hydrol. Process.*, vol. 25, no. 1, pp. 152–158, 2011.

[73] M. R. Turetsky, R. K. Wieder, C. J. Williams, and D. H. Vitt, "Organic matter accumulation, peat chemistry, and permafrost melting in peatlands of boreal Alberta," *Ecoscience*, vol. 7, no. 3, pp. 379–392, 2000.

[74] S. Payette, A. Delwaide, M. Caccianiga, and M. Beauchemin, "Accelerated thawing of subarctic peatland permafrost over the last 50 years," *Geophys. Res. Lett.*, vol. 31, 2004, Art.ID. L18208.

[75] E. S. Kasischke and L. L. Bourgeau-Chavez, "Monitoring south Florida wetlands using ERS-1 SAR imagery," *Photogramm. Eng. Remote Sens.*, vol. 63, no. 3, pp. 281–291, 1997.

[76] E. Kasischke, K. Smith, L. Bourgeau-Chavez, E. Romanowicz, S. Brunzell, and C. Richardson, "Effects of seasonal hydrologic patterns in south Florida wetlands on radar backscatter measured from ERS-2 SAR imagery," *Remote Sens. Environ.*, vol. 88, pp. 423–441, 2003.

[77] E. Kasischke, L. Bourgeau-Chavez, A. Rober, K. Wyatt, J. Waddington, and M. Turetsky, "Effects of soil moisture and water depth on ERS SAR backscatter measurements from an Alaskan wetland complex," *Remote Sens. Environ.*, vol. 113, pp. 1868–1873, Sep. 2009.

[78] L. Bourgeau-Chavez, K. Smith, S. Brunzell, C. Richardson, E. Romanowicz, and E. Kasischke, "Remote monitoring of regional scale inundation patterns and hydroperiod in the Greater Everglades using synthetic aperture radar," *Wetlands*, vol. 25, pp. 176–191, 2005.

[79] Y. Maghsoudi, M. J, Collins, and D. G. Leckie, "Radarsat-2 polarimetric SAR data for boreal forest classification using SVM and a wrapper feature selector," *IEEE J. Sel. Topics Appl. Earth Observ. Remote Sens.*, vol. 6, no. 3, pp. 1531–1538, Jun. 2013.

Michael A. Merchant received the M.Sc. degree from the University of Guelph, Guelph, Canada, in 2012.

He is currently working as a Remote Sensing Specialist with Ducks Unlimited Canada (DUC), Boreal Program, Edmonton, AB, Canada, where he leads the development of numerous DUC wetland inventory mapping projects using synthetic aperture radar and multispectral satellite imagery. His research interests include land cover classification, wetland hydrology, sensor fusion, and image interpretation.

Justin R. Adams received the B.A. degree in geographic analysis from Ryerson University, Toronto, ON, Canada, and the M.Sc. and Ph.D. degrees in physical geography from the University of Guelph, Guelph, ON, Canada.

He is currently a Postdoctoral Fellow in the Cold Regions Research Centre, Wilfrid Laurier University, Waterloo, ON, Canada. His current research interest focuses on remote sensing and hydrological modeling of forest and wetland land covers over discontinuous permafrost environment using multispectral and radar datasets.

Aaron A. Berg received the B.Sc. and M.Sc. degrees in geography from the University of Lethbridge, Lethbridge, AB, Canada, the M.S. degree in geological sciences from the University of Texas at Austin, Austin, TX, USA, and the Ph.D. degree in earth system science from the University of California at Irvine, Irvine, CA, USA.

He is currently a Professor and the Canada Research Chair in hydrology and remote sensing in the Department of Geography, University of Guelph, Guelph, ON, Canada. He teaches physical geography, hydrology, and remote sensing. His research interests include hydrological modeling and terrestrial remote sensing.

William L. Quinton has studied in the Canadian Arctic since 1987, and in the Taiga Plains since 1991.

He is an Associate Professor in the Department of Geography and Environmental Studies, Wilfrid Laurier University, Waterloo, ON, Canada. In 1999, he established the Scotty Creek Research Station, where he has led several major research studies in the southern Northwest Territories focused on the impacts of permafrost thaw on basin hydrology and ecosystems. As part of these studies, he has drawn to Scotty Creek, a world-class interdisciplinary research team to address complex scientific questions on how climate warming affects northern ecosystems. He has served as the Co-Director of the Cold Regions Research Centre, and recently also served as the President of the Canadian Geophysical Union-Hydrology Section, and National Representative to the International Association of Hydrological Sciences, and to the Northern Research Basins Working Group.

Jennifer L. Baltzer received the B.Sc. degree in biology from Acadia University, Wolfville, NS, Canada, and the Ph.D. degree in forestry from the University of Toronto, Toronto, ON, Canada.

She is an Associate Professor and the Canada Research Chair in forests and global change in the Biology Department, Wilfrid Laurier University, Waterloo, ON, Canada. Her research focuses on the impacts of climate warming on forest ecosystems globally including boreal peatland systems in the North.

Laura E. Chasmer received the B.E.S. and M.E.S. degrees in geography from the University of Waterloo, Waterloo, ON, Canada, and the Ph.D. degree in geography from Queen's University, Kingston, ON, Canada.

She is currently an Assistant Professor in physical geography with the University of Lethbridge, Lethbridge, AB, Canada. Her research interests include fusion of *in situ* hydro-meteorological data and remote sensing change detection using airborne LiDAR and optical imagery within Boreal forest and wetland environment.